CMF models of hot star winds

I. Test of the Sobolev approximation in the case of pure line transitions

J. Krtička[1] and J. Kubát[2]

[1] Ústav teoretické fyziky a astrofyziky PřF MU, CZ-611 37 Brno, Czech Republic, e-mail: `krticka@physics.muni.cz`
[2] Astronomický ústav, Akademie věd České republiky, CZ-251 65 Ondřejov, Czech Republic

ABSTRACT

We provide hot star wind models with radiative force calculated using the solution of comoving frame (CMF) radiative transfer equation. The wind models are calculated for the first stars, O stars, and the central stars of planetary nebulae. We show that without line overlaps and with solely thermal line broadening the pure Sobolev approximation provides a reliable estimate of the radiative force even close to the wind sonic point. Consequently, models with the Sobolev line force provide good approximations to solutions obtained with non-Sobolev transfer. Taking line overlaps into account, the radiative force becomes slightly lower, leading to a decrease in the wind mass-loss rate by roughly 40%. Below the sonic point, the CMF line force is significantly lower than the Sobolev one. In the case of pure thermal broadening, this does not influence the mass-loss rate, as the wind mass-loss rate is set in the supersonic part of the wind. However, when additional line broadening is present (e.g., the turbulent one) the region of low CMF line force may extend outwards to the regions where the mass-loss rate is set. This results in a decrease in the wind mass-loss rate. This effect can at least partly explain the low wind mass-loss rates derived from some observational analyses of luminous O stars.

Key words. stars: winds, outflows – stars: mass-loss – stars: early-type – hydrodynamics – radiative transfer

1. Introduction

One of the most important galactic populations consists of massive stars, because these stars dominate the spectra of many galaxies and contribute significantly to the mass and momentum input into the interstellar matter. Moreover, massive stars end their active lives in gigantic explosions such as supernovae or even possibly as the progenitors of gamma-ray bursts (see Woosley & Heger 2006, Yoon & Langer 2005), producing huge amounts of heavier elements.

An important property of hot stars that significantly influences their final stages is the stellar wind (see, e.g., Owocki 2004, Krtička & Kubát 2007a, Puls et al. 2008b, for reviews dedicated to hot star winds). However, in stellar evolution calculations it is usually unnecessary to know detailed wind properties, but just the amount of mass expelled from the star per unit of time (mass-loss rate) as a function of stellar parameters (e.g., mass, effective temperature, radius, surface metallicity). However, for many hot stars we simply cannot estimate their true mass-loss rate with the precision necessary to calculate evolutionary models. The situation may be less problematic for luminous O stars, for which relatively good agreement between theoretical predictions and observational results seems to exist (Pauldrach et al. 2001, Vink et al. 2001, Krtička & Kubát 2004, hereafter Paper I).

However, the agreement between theoretically predicted mass-loss rates and those derived from observations may be an illusion caused by the neglect of some physical effects in the wind, such as clumping (Bouret et al. 2003, Martins et al. 2005). As a result, the true mass-loss rates

of O stars may be a few times lower than the standard wind theory predicts. This seems to be supported by the observations of Fullerton et al. (2006) of weak wind line profiles of P V. Last but not least, the unexpected occurrence of symmetrical X-ray line profiles seems to require relatively low wind mass-loss rates (Kramer et al. 2003).

Possibly unreliable estimates of hot star wind mass-loss rates are also problematic because altough more realistic evolutionary stellar models can be calculated, by including, e.g., rotation and magnetic fields, the wind mass-loss rates remain uncertain. Ideally, all observational indicators of mass-loss rate and theoretical models should find and predict similar mass-loss rates. From the observational point of view, more detailed models of line formation in inhomogeneous media may be necessary to obtain reliable line profiles, and consequently also estimate mass-loss rates (Oskinova et al. 2007, Sundqvist et al. 2010).

From the theoretical point of view, disagreement between theory and observations would imply that some of the assumptions used for the hot-star wind modeling are inaccurate. Part of the disagreement may be caused by using incorrect abundances (Krtička & Kubát 2007b), although the reason for a disagreement remains mainly unclear. A thorough inspection of all assumptions involved in the modeling is therefore strongly needed. As a first step in this direction, we studied the influence of X-rays on the wind structure of hot stars. It seems that X-rays alone cannot entirely explain the disagreement between theory and observations (Krtička & Kubát 2009) as their influence on wind mass-loss rates is small and they do not strongly affect the ionization fraction of many important ions, especially that of P V. On the other hand, the modified

ionization equilibrium may affect the X-ray line formation (Oskinova et al. 2006, Krtička & Kubát 2009), and too ling cooling time in the post-shock region (Cohen et al. 2008, Krtička & Kubát 2009) may cause the so-called "weak wind problem" (Bouret et al. 2003, Martins et al. 2004, Marcolino et al. 2009).

One of the most important approximations in the hot-star wind modeling is the Sobolev approximation (Sobolev 1947, Castor 1974), which enables us to solve the line radiation transfer analytically. Some studies confirm its applicability in the supersonic part of smooth line-driven winds (Hamann 1981, Pauldrach et al. 1986, Puls 1987). However, the applicability of the Sobolev approximation is questionable especially in the regions close to the photosphere because of the existence of strong source function gradients (Owocki & Puls 1999). On the other hand, some models avoid using the Sobolev approximation and use only the comoving-frame (hereafter CMF) method of solving the radiative transfer equation (e.g., Gräfener & Hamann 2005).

We decided to test the applicability of the Sobolev approximation and include the CMF solution of the radiative transfer equation in our wind models. In this first paper of a series, we describe our method, and study the applicability of the Sobolev approximation using models neglecting continuum opacity.

2. Basic model assumptions

The models used in this paper are based on the NLTE wind models of Krtička & Kubát (2004, hereafter Paper I). Here we summarise only their basic features and describe the inclusion of CMF line force.

We assume a spherically symmetric stationary stellar wind. The excitation and ionization state of the considered elements is derived from the statistical equilibrium (NLTE) equations. Ionic models are either adopted from the TLUSTY grid of model stellar atmospheres (Lanz & Hubeny 2003, 2007) or are prepared by us using the data from the Opacity and Iron Projects (Seaton 1987, Fernley et al. 1987, Luo & Pradhan 1989, Sawey & Berrington 1992, Seaton et al. 1992, Butler et al. 1993, Nahar & Pradhan 1993, Hummer et al. 1993, Bautista 1996, Nahar & Pradhan 1996, Zhang 1996, Bautista & Pradhan 1997, Zhang & Pradhan 1997, Chen & Pradhan 1999). As in Paper I, the solution of the radiative transfer equation for NLTE equations is artificially split into two parts, namely the radiative transfer in either the continuum or in lines. The solution to the radiative transfer equation in continuum is based on the Feautrier method in the spherical coordinates (Mihalas & Hummer 1974, Kubát 1993), and the line radiative transfer is solved in the Sobolev approximation (Castor 1974, Rybicki & Hummer 1978) neglecting continuum opacity and line overlaps.

In contrast to our previous models, the radiative transfer in lines used for the calculation of the radiative force is solved in the CMF (see Sect. 3) neglecting the continuum opacity. The line radiative force is calculated directly from the true chemical composition, NLTE ionization and excitation balance, and CMF flux using data from the VALD database (Piskunov et al. 1995, Kupka et al. 1999). We do not use the line-strength distribution function parameterized by force multipliers k, α, and δ.

The flux at the surface (used as the lower boundary condition for the radiative transfer in the wind) is taken from the H-He spherically symmetric NLTE model stellar atmospheres of Kubát (2003, and references therein).

3. CMF calculation of the radiative force

The radiative force is calculated using the solution of the spherically symmetric CMF radiative transfer equation (Mihalas 1978, Eq. (14.99))

$$\mu \frac{\partial I(\nu, \mu, r)}{\partial r} + \frac{1 - \mu^2}{r} \frac{\partial I(\nu, \mu, r)}{\partial \mu}$$
$$- \frac{\nu v_r}{cr} \left[1 - \mu^2 + \mu^2 \frac{r}{v_r} \frac{\mathrm{d}v_r}{\mathrm{d}r} \right] \frac{\partial I(\nu, \mu, r)}{\partial \nu}$$
$$= \eta(\nu, r) - \chi(\nu, r) I(\nu, \mu, r), \quad (1)$$

where $I(\nu, \mu, r)$ is the intensity seen by the observer moving with the wind at the radial velocity v_r, ν is the frequency, $\mu = \cos\theta$, θ is the direction between the given ray and the radial direction, and $\eta(\nu, r)$ and $\chi(\nu, r)$ are the line emissivity and opacity, respectively, given by

$$\eta(\nu, r) = \frac{2h\nu^3}{c^2} \sum_{i,j} \frac{\pi e^2}{m_e c} \frac{n_j}{g_j} g_i f_{ij} \varphi_{ij}(\nu), \quad (2a)$$

$$\chi(\nu, r) = \sum_{i,j} \frac{\pi e^2}{m_e c} \left(\frac{n_i}{g_i} - \frac{n_j}{g_j} \right) g_i f_{ij} \varphi_{ij}(\nu), \quad (2b)$$

where n_i and n_j are the number densities of individual states with statistical weights g_i and g_j corresponding to the line transition $i \leftrightarrow j$ with oscillator strength f_{ij} and the line-profile $\varphi_{ij}(\nu)$, and m_e is the electron mass. Assuming the line profile to be Gaussian produced by thermal broadening only, $\varphi_{ij}(\nu)$ is given by

$$\varphi_{ij}(\nu) = \frac{1}{\sqrt{\pi}\Delta\nu_{ij}} \exp\left[\frac{(\nu - \nu_{ij})^2}{\Delta\nu_{ij}^2} \right], \quad (3)$$

where ν_{ij} is the laboratory line frequency, and the line broadening is given by

$$\Delta\nu_{ij} = \frac{\nu_{ij}}{c} \sqrt{\frac{2kT}{m_a}}, \quad (4)$$

and m_a is the mass of a given atom. The number densities of individual levels in Eqs. (2) are calculated from statistical equilibrium (NLTE) equations.

Writing Eq. (1), we neglected advection and aberration terms, which is justifiable in non-relativistic flows (see, e.g., Korčáková & Kubát 2003). We also note that by neglecting the spatial derivatives of intensity in Eq. (1) we obtain the Sobolev approximation (Castor 2004).

Following Mihalas et al. (1975), we rewrite Eq. (1) for rays with an impact parameter p

$$\pm \frac{\partial I^\pm(\nu, p, z)}{\partial z} - \frac{\nu v_r}{cr} \left[1 - \mu^2 + \mu^2 \frac{r}{v_r} \frac{\mathrm{d}v_r}{\mathrm{d}r} \right] \frac{\partial I^\pm(\nu, p, z)}{\partial \nu}$$
$$= \eta(\nu, r) - \chi(\nu, r) I^\pm(\nu, p, z), \quad (5)$$

where $+$ and $-$ refers to radiation flowing toward and away from the observer, respectively, $r = (p^2 + z^2)^{1/2}$, and z

is the distance along the ray. We transform Eq. (5) using intensity-like and flux-like variables

$$u(\nu, p, z) = \frac{1}{2} \left[I^+(\nu, p, z) + I^-(\nu, p, z) \right], \quad (6a)$$

$$v(\nu, p, z) = \frac{1}{2} \left[I^+(\nu, p, z) - I^-(\nu, p, z) \right], \quad (6b)$$

to obtain a system of partial differential equations

$$\frac{1}{\chi(\nu, r)} \frac{\partial u(\nu, p, z)}{\partial z} - \gamma(\nu, p, z) \frac{\partial v(\nu, p, z)}{\partial \nu} = -v(\nu, p, z), \quad (7a)$$

$$\frac{1}{\chi(\nu, r)} \frac{\partial v(\nu, p, z)}{\partial z} - \gamma(\nu, p, z) \frac{\partial u(\nu, p, z)}{\partial \nu} = S(\nu, r) - u(\nu, p, z), \quad (7b)$$

where

$$\gamma(\nu, p, z) = \frac{\alpha(r)}{r\chi(\nu, r)} \left[1 - \mu^2 + \beta(r)\mu^2 \right], \quad (8)$$

$$\alpha(r) = \frac{\nu v_r}{c}, \quad (9)$$

$$\beta(r) = \frac{r}{v_r} \frac{dv_r}{dr}, \quad (10)$$

$$S(\nu, r) = \frac{\eta(\nu, r)}{\chi(\nu, r)}. \quad (11)$$

The system of equations in Eq. (7) is solved numerically using the long characteristic method of Mihalas et al. (1975), which we modified slightly for the present purpose (see Appendix A). As we are interested in the calculation of the radiative force using the v variable at a particular grid point, in contrast to Mihalas et al. (1975) we specify v at grid points, and u in the middle between them.

In our numerical solution of Eq. (7), we use the same spatial grid as for the solution of hydrodynamical equations. The spacing of the frequency grid is $\Delta\nu_D = \nu\sqrt{(2kT_C/m_C)}/(cf_D)$, where T_C is the pre-specified expected minimum wind temperature, m_C is the atomic mass of artificial metallic atom, and f_D is the multiplicative factor (see below). The CMF radiative transfer equation is solved only for selected frequencies from the frequency grid that lie close to some line. The selection of frequencies is controlled by two integer numbers n_D, and NCERV (cf. Hillier & Miller 1998). For each line, we select frequencies that lie within n_D line Doppler widths $\Delta\nu_{ij}$. Redward of the center of each line, we select each NCERV frequency up to the frequency corresponding to the Doppler shift for the wind terminal velocity. The numerical test showed that a sufficiently precise value of the radiative force can be derived for the value of parameters $m_C = 60\,m_H$, where m_H is the mass of hydrogen atom, $f_D = 2$, $n_D = 5$, NCERV=30, and typically $T_C = 10\,000 - 20\,000$ K.

The radiative force is calculated as an integral

$$f_{rad}^{CMF} = \frac{1}{c} \int_0^\infty \chi(\nu, r) F(\nu, r)\, d\nu$$
$$= \frac{4\pi}{c} \int_0^\infty d\nu \int_0^1 d\mu\, \mu\chi(\nu, r)v(\nu, p, z). \quad (12)$$

As the calculation of the CMF radiative force is rather time-consuming, we do not calculate f_{rad}^{CMF} during each iteration of hydrodynamical variables, but adopt a different approach. We calculate the ratio of the CMF and Sobolev line forces

$$c^{CMF} = \frac{f_{rad}^{CMF}}{f_{rad}^{Sob}}. \quad (13)$$

By the Sobolev line force f_{rad}^{Sob}, we mean here the force calculated by assuming the Sobolev approximation for radiative transfer, neglecting line overlaps and using true line opacities and the emergent flux from the underlying stellar atmosphere (Paper I, Eq. (25) therein). Unless the base density is known with a precision better than about 30%, we calculate c^{CMF} only when the estimate of the base density is changed, and keep c^{CMF} fixed during the subsequent iterations of the hydrodynamical structure. When the base density is known with a higher precision, we calculate c^{CMF} after each change of the hydrodynamical structure. Moreover, because we solve the hydrodynamical equations using the Newton-Raphson method, we have to calculate the derivatives of f_{rad}^{CMF} with respect to individual hydrodynamical variables. These derivatives are approximated using the derivatives of the Sobolev line force f_{rad}^{Sob} multiplied by c^{CMF}. The force term in the critical point condition (see Paper I) is also multiplied by c^{CMF}.

We note that direct use of Eq. (13) causes instability in the model convergence. The reason for these convergence problems may be numerical, but this behavior may also be connected with line-driven instability (Owocki et al. 1988, Feldmeier et al. 1997). To avoid this (since we are seeking stationary solution and not evolution with time) we introduced a weak smoothing of c^{CMF},

$$\bar{c}_d^{CMF} = \frac{1}{4} \left(2c_d^{CMF} + c_{d-1}^{CMF} + c_{d+1}^{CMF} \right), \quad (14)$$

where c_d^{CMF} is the value of c^{CMF} at a given grid point d (as for $d-1$ and $d+1$) and we use $\bar{c}_d^{CMF}$ instead of c_d^{CMF} in the models. Our numerical tests showed that the smoothing Eq. (14) does not significantly affect the resulting radiative force.

4. Studied model stars

In our study, we selected three types of stars to study more carefully the Sobolev approximation in different wind environments (see Table 1).

The stellar parameters of the first stars were obtained according to an evolutionary calculation of initially zero-metallicity star with initial mass $50\,M_\odot$ derived by Marigo et al. (2001). For these models, we assumed a stellar wind driven purely by CNO elements (which appear on the stellar surface due to mixing) with a mass-fraction of CNO $Z = 10^{-3}$.

The stellar parameters (effective temperatures and radii) of an O star sample were derived using the model atmospheres with line blanketing (Repolust et al. 2004, Markova et al. 2004, Martins et al. 2005). Stellar masses were obtained using evolutionary tracks either by ourselves (using Schaller et al. 1992 tracks) or by Martins et al. (2005). For these stars, we assumed a solar chemical composition (Asplund et al. 2005).

The stellar parameters of central stars of planetary nebulae were taken from Pauldrach et al. (2004), who derived them from UV spectroscopy. Helium abundance was adopted from Kudritzki et al. (1997), for other elements we

Table 1. Radius R_*, mass M, and the effective temperature T_{eff} of studied model stars

Star (model)		R_* [$R_\odot$]	M [$M_\odot$]	T_{eff} [K]
First stars				
M500-1		11.1	50	50 000
M500-2		33.7	50	29 900
M500-3		72.0	50	20 600
M500-4		303	50	10 100
O stars				
ξ Per	HD 24912	14.0	36	35 000
ι Ori	HD 37043	21.6	41	31 400
15 Mon	HD 47839	9.9	32	37 500
	HD 54662	11.9	38	38 600
	HD 93204	11.9	41	40 000
ζ Oph	HD 149757	8.9	21	32 000
68 Cyg	HD 203064	15.7	38	34 500
19 Cep	HD 209975	22.9	47	32 000
Central stars of planetary nebulae				
NGC 2392		1.5	0.41	40 000
NGC 3242		0.3	0.53	75 000
IC 4637		0.8	0.87	55 000
IC 4593		2.2	1.11	40 000
He 2-108		2.7	1.33	39 000
IC 418		2.7	1.33	39 000
Tc 1		3.0	1.37	35 000
NGC 6826		2.2	1.40	44 000
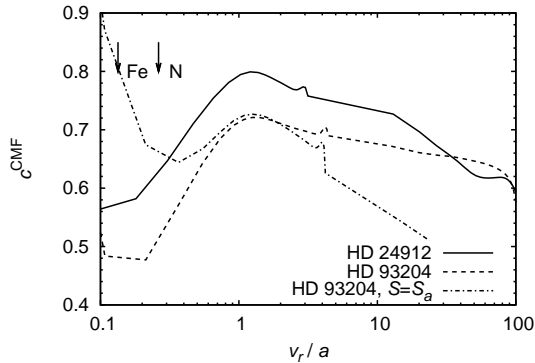
Fig. 1. The ratio of the CMF to Sobolev line forces given by Eq. (13) as a function of the wind velocity plotted in the terms of the sound speed for two selected stars. The dashed-dotted line denotes a model with constant source function and constant level populations equal to their values at the sonic point. Arrows indicate the thermal speed of selected ions.

assumed a solar chemical composition (after Asplund et al. 2005), which was for some stars slightly modified according to Pauldrach et al. (2004).

5. Comparison of CMF and Sobolev wind models

We calculated wind models with both CMF and Sobolev line forces and compared the final wind structure. The resulting ratio of the CMF to Sobolev line forces c^{CMF} for selected stars is shown in Fig. 1. We note that the Sobolev force was calculated using the flux from the stellar atmosphere and by neglecting line overlaps.

For very low wind velocities $v_r \lesssim 0.1a$ (where $a^2 = 2kT/m_{\text{H}}$), the CMF force is large, $c^{\text{CMF}} > 1$. This is most likely partly connected with the boundary conditions, which are not completely compatible with the wind (cf., Noerdlinger & Rybicki 1974).

For velocities of about one tenth of the sound speed, there is an apparent minimum of c^{CMF}. In some cases, the ratio c^{CMF} could even be negative, which corresponds to a negative CMF radiative force. The Sobolev approximation is not applicable in this region, but a low value of the radiative force is also connected with positive source function gradients. For subsonic velocities, the Doppler shift is less important, and the line radiative transfer is given basically by the static radiative transfer equation. In the optically thick regions, for frequencies corresponding to line transitions it follows from Eq. (7b) $u \approx S$, from Eq. (7a) $v \approx -(1/\chi)\mathrm{d}S/\mathrm{d}z$, and the radiative force is proportional to the negative of the derivative of the source function $f_{\text{rad}}^{\text{CMF}} \sim -\mathrm{d}S/\mathrm{d}z$ (see Eq. (12), and Noerdlinger & Rybicki 1974). Because the line source function increases here (see Fig. 2), the line radiative force at low velocities may even be negative. For a constant source function, the minimum of c^{CMF} close to the star is significantly weaker (see Fig. 1). The source function minimum below the sonic point is caused by a local temperature minimum, because the line source function of optically thick lines (which are, consequently, in detailed radiative balance) close to the star $S \approx n_j/n_1 \sim (n_j/n_1)^*$ (asterisk denotes LTE value) depends on temperature. Another source function minimum for non-Sobolev source function due to velocity field curvature was also found by Sellmaier et al. (1993), and Owocki & Puls (1999). We note that in the case of the resonance lines plotted in Fig. 2 the line source function at larger radii is roughly proportional to $S \sim n_j/n_1 \sim r^{-3}$ (e.g., Kudritzki & Puls 2000).

The minimum of c^{CMF} close to the star is also connected with the velocity gradient changing significantly within the resonance zone. Thus, a given line also picks up the radiation corresponding to a lower velocity gradient leading to a further reduction in the radiative force. For velocities comparable to or higher than the ion thermal speed, the lines are deshadowed because of the Doppler effect, and the radiative force increases. We note that we only include the thermal broadening, hence these effects occur for velocities lower than the sound speed.

As the wind accelerates, the ratio of the CMF to Sobolev line force increases and reaches a value close to one for velocities higher than the thermal speed of the wind driving ions (Fig. 1). This is unsurprising, because the Sobolev approximation is applicable to regions with a large velocity gradient, which exist already close to the sonic point $v_r = a$. Owing to line overlaps, c^{CMF} is less than one in the outer wind regions, where it reaches only $0.7 - 0.8$.

To test the influence of line overlaps, we calculated the radiative force with only 50 carefully selected optically thick lines that do not overlap (see Fig. 3). The pronounced minimum for velocities lower than the sound speed is still present here, but in the outer regions the value of c^{CMF} is approximately one, supporting the validity of the Sobolev approximation for supersonic velocities.

To understand more clearly the influence of line overlaps on the radiative force, we constructed another artificial line list using our set of non-overlapping lines. Each line in this new line list is counted twice with all parameters being
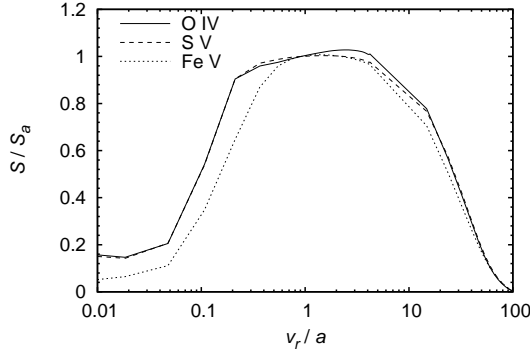
Fig. 2. The line source function for resonance lines of O IV at 790 Å, S V at 786 Å, and Fe V at 388 Å as a function of relative wind velocity. The source function is plotted relative to its value at the sonic point S_a for the wind model of HD 93204.
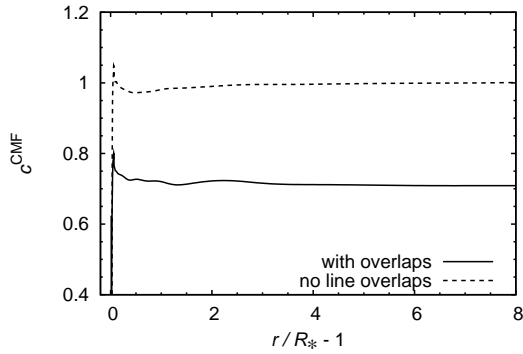
Fig. 3. The radial variation in the ratio of the CMF to Sobolev line forces in the wind model of Tc 1 central star with and without line overlaps.
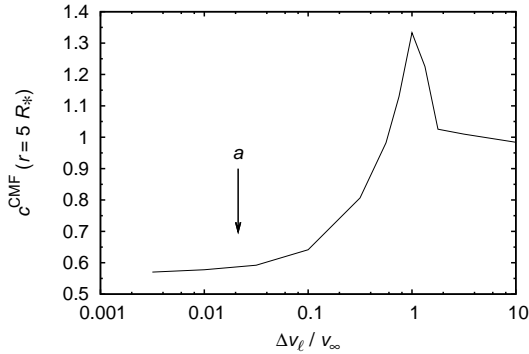
Fig. 4. The ratio of the CMF to Sobolev line forces at radius $r = 5\,R_*$ in the Tc1 wind model in the dependence on the line shift. The value of hydrogen thermal speed is denoted in the figure.

completely the same, however with a line center shifted by $\nu_{ij}\Delta v_\ell/c$, where Δv_ℓ is a free parameter. For $\Delta v_\ell \ll a$, all twin lines completely overlap leading to a significant decrease in the radiative force with respect to the Sobolev one that does not account for the line overlaps (see Fig. 4). For $\Delta v_\ell > a$, the lines at a given point do not overlap, but one of the twin lines "sees" the flux absorbed by the

Table 2. Comparison of calculated wind parameters derived using CMF and Sobolev line forces

Star	$\dot{M}^{\mathrm{Sob}}$ [M$_\odot$ year^{-1}]	v_∞^{Sob} [km s^{-1}]	$\dot{M}^{\mathrm{CMF}}$ [M$_\odot$ year^{-1}]	v_∞^{CMF} [km s^{-1}]
First stars				
M500-1	6.3×10^{-08}	2750	6.1×10^{-08}	4010
M500-2	4.0×10^{-07}	1930	2.0×10^{-07}	1310
M500-3	2.1×10^{-07}	580	1.4×10^{-07}	790
M500-4	3.8×10^{-08}	600	2.8×10^{-08}	620
O stars				
HD 24912	4.4×10^{-7}	2270	2.3×10^{-7}	2030
HD 37043	6.2×10^{-7}	2340	4.1×10^{-7}	2000
HD 47839	2.2×10^{-7}	3080	1.0×10^{-7}	2970
HD 54662	7.9×10^{-7}	2190	4.1×10^{-7}	2050
HD 93204	1.3×10^{-6}	2290	5.9×10^{-7}	2080
HD 149757	4.7×10^{-8}	2040	2.9×10^{-8}	1860
HD 203064	5.7×10^{-7}	2080	3.8×10^{-7}	1780
HD 209975	8.4×10^{-7}	2430	5.5×10^{-7}	1960
Central stars of planetary nebulae				
NGC 2392	3.7×10^{-8}	490	1.8×10^{-8}	500
NGC 3242	3.1×10^{-9}	2000	2.0×10^{-9}	1890
IC 4637	3.1×10^{-8}	1440	1.4×10^{-8}	1270
IC 4593	7.4×10^{-8}	730	3.8×10^{-8}	660
He 2-108	9.5×10^{-8}	730	4.7×10^{-8}	700
IC 418	9.5×10^{-8}	730	4.7×10^{-8}	700
Tc 1	2.8×10^{-8}	870	1.8×10^{-8}	800
NGC 6826	1.8×10^{-7}	870	7.6×10^{-8}	790

second line, leading to a reduction in the radiative force even in this case. For $\Delta v_\ell \approx v_\infty$, one of the lines is affected by the emission from the second one, leading to an increase in the CMF radiative force relative to the Sobolev one.

A similar reduction in the line force by multiline effects was found by Puls (1987). We note that the multiline effects were also studied with respect to the multiple radiative momentum deposition in Wolf-Rayet star winds (Gayley et al. 1995). However, these effects are probably of minor importance here due to the low density of the studied winds.

The CMF radiative force, which is lower than the Sobolev one because of line overlaps, causes a decrease in the mass-loss rate of CMF models with respect to Sobolev ones (see Table 2). The ratio of CMF to Sobolev mass-loss rates is about 0.58. The only exception is the model M500-1, for which the CMF mass-loss rate is nearly the same as the Sobolev one. The reason is that the star is so hot, that the wind is accelerated mainly by a dozen O V and O VI lines. For a critical point velocity, these lines do not overlap, hence $c^{\mathrm{CMF}} \approx 1$, and the CMF and Sobolev mass-loss rates are nearly the same.

The resulting wind parameters of the central stars of planetary nebulae can be compared with those derived from observations by Pauldrach et al. (2004, see Fig. 5). There is reasonable agreement between the wind parameters predicted by ourselves and those derived by Pauldrach et al. (2004, see Fig. 5). The mass-loss rates of Pauldrach et al. (2004) are on average a factor of about 1.6 higher than those derived by ourselves. This is most likely partly because of the simplifications included in our code, e.g., the neglect of continuum opacity sources, and partly by the different abundances adopted.
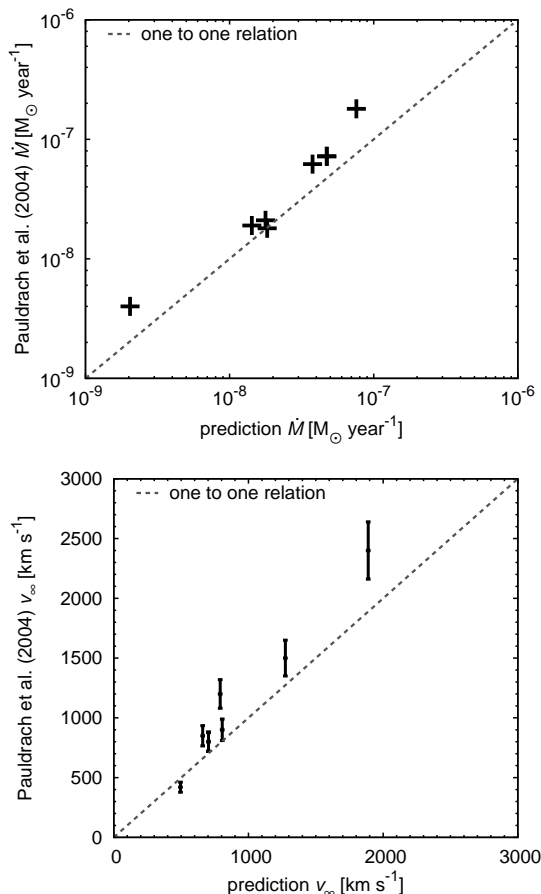
Fig. 5. Comparison of our derived mass-loss rates (upper panel) and terminal velocities (lower panel) of the central stars of planetary nebulae with those derived by Pauldrach et al. (2004).
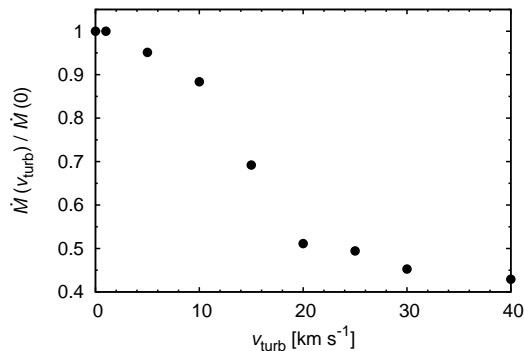
Fig. 6. The mass-loss rate of HD 209975 in the models with additional turbulent line broadening relative to the models with zero turbulent velocity.

6. Models with base turbulence

The existence of a region close to the stellar surface where the CMF line force is low compared to the Sobolev one (see Fig. 1) is partly caused by the source function gradients at the wind base and partly by the Sobolev approximation not being applicable to the subsonic regions. The CMF line force increases at the moment when the line starts to absorb the radiation that has not been absorbed yet, i.e., the

radiation from the line wing. Because up to now we have assumed pure thermal line broadening, the velocity width of low CMF line force is of the order of the metallic thermal speed (which is roughly $0.13a$ in the case of iron). The wind mass-loss rate in our models is determined in the region of supersonic wind, close to the critical point where the wind velocity approaches the speed of radiative-acoustic waves (Abbott 1980, Feldmeier et al. 2008). Thus, the region of low CMF line force close to the star does not significantly affect the wind mass-loss rate.

However, if the line broadening were larger (due to surface turbulence), then the region of low CMF line force could spread out to large velocities comparable to the turbulent one. When the turbulent velocity is comparable to the critical point velocity, below which the wind mass-loss rate is set, this could cause a significant decrease in the wind mass-loss rate. To test this, we calculated wind models with additional line broadening, which we attributed to the turbulent one. In this case, the line profile width is given not by Eq. (4), but by

$$\Delta\nu_{ij} = \frac{\nu_{ij}}{c}\sqrt{v_{\mathrm{turb}}^2 + \frac{2kT}{m_a}}, \qquad (15)$$

where v_{turb} is the adopted turbulent velocity.

The results of numerical models indicate that with increasing turbulent broadening the velocity width of low CMF line force increases leading to a lower mass-loss rate (see Fig. 6, cf. Lucy 2007). Hence, in the presence of turbulence the wind parameters may not depend only on the basic stellar parameters (effective temperature, radius, mass) but also on the line turbulent broadening. Moreover, this effect can possibly be one of the reasons why the mass-loss rates derived from observational analyses that take the clumping into account (Bouret et al. 2003, Martins et al. 2005) are systematically lower than the predicted ones.

For velocities higher than a few times the turbulent one, the Sobolev approximation should be applicable. At these high velocities, one expects that the line force becomes close to the Sobolev one. Because now the same force (as in the model with zero turbulent broadening) accelerates the wind of lower density, one expects the terminal velocity to increase (e.g., Gayley 2001), becoming much higher than the observed one. However, our models do not predict a significant increase in the terminal velocity v_∞, which is in the range $1900-2200\,\mathrm{km\,s^{-1}}$ for the wind models of HD 209975 with different turbulent broadening. This is caused by the stronger blocking of stellar radiation by increased line overlaps mainly in the region with $v_r \lesssim a$. We note that lines broadened by turbulent motions are able to block the flux more efficiently than lines broadened purely thermally.

Observational studies consider the turbulence already present in the photospheres of O stars (e.g., Bouret et al. 2003, 2005, Martins et al. 2004, 2005) with turbulent velocities of about $2-25\,\mathrm{km\,s^{-1}}$. Macroturbulent velocities in B supergiants may be even higher, about $30-100\,\mathrm{km\,s^{-1}}$ (Howarth et al. 1997, Markova & Puls 2008). Convective layers and surface pulsational motions are also expected theoretically (Cantiello et al. 2009, Aerts et al. 2009). Turbulence can spread in the wind (Feldmeier et al. 1997), leading to a decrease in the wind mass-loss rate, as shown here. We also note that many O stars exhibit turbulent velocities in the range $10-20\,\mathrm{km\,s^{-1}}$, where we expect a high sensitivity of the predicted mass-loss rate to the turbulent velocity (see Fig. 6).
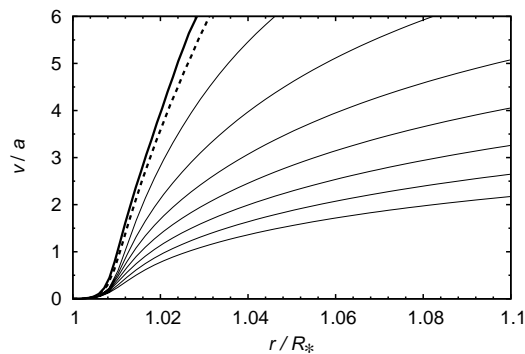
Fig. 7. The dependence of the radial velocity on radius for solutions with different boundary densities (mass-loss rates) close to the stellar surface for the model star 500-1. Each consecutive model (from down to up) differs by a factor of 1.5 in the mass-loss rate (thin lines). The thick line denotes the unique solution that smoothly intercepts the critical point. The dashed line denotes solution with the Sobolev line force.

The basic results presented here will, in the future, be tested in more detail using models that also account for the continuum opacity and CMF line source function in a separate study.

7. The solution topology

In Fig. 7, we plot solutions with different base densities (mass-loss rates). In generall, with increasing base density the wind velocity increases until the density reaches a maximum value. There is no solution that is smooth out to large radii for the densities higher than the maximum one. The solution with maximum density is very similar to the critical solution of Sobolev models (see Fig. 7). Moreover, there are many solutions that smoothly pass through the sonic point $v = a$ for different mass-loss rates.

This indicates that the critical point of non-Sobolev models is close to the CAK critical point (Castor, Abbott & Klein 1975) and that the sonic point is *not* a point where the wind mass-loss rate is determined. The reason is that even in the non-Sobolev models the radiative force is not given locally by wind density and velocity, but depends on the wind properties in a close neighborhood of a studied point. This dependence on the non-local properties at its limit approaches the Sobolev approximation for very thin resonance layers (for very large velocity gradients).

8. Conclusions

We have presented hot star wind models in which the radiative force is calculated using the solution of the comoving frame (CMF) radiative transfer equation. The wind models were calculated for three different groups of stellar parameters (corresponding to evolved first stars, O stars, and the central stars of planetary nebulae) to compare the CMF and Sobolev radiative forces for a broader range of stellar parameters.

The comparison of the CMF radiative force with an approximate one calculated by assuming the Sobolev approximation showed that the Sobolev line force is slightly higher

due to the neglect of line overlaps. Thus, the mass-loss rate of wind models that include the Sobolev line force is on average a factor of about 1.7 higher than a more realistic one calculated using CMF wind models. However, we note that the simple Sobolev approximation applied here for reference can be improved to account for line overlaps and continuum absorption (Olson 1982, Hummer & Rybicki 1985, Puls & Hummer 1988, Pavlakis & Kylafis 1996). We emphasize that modern hot star wind models include line overlaps (e.g., Vink et al. 2001, Pauldrach et al. 2001, Gräfener & Hamann 2005).

Without line overlaps in the case of purely thermal line broadening, the Sobolev approximation provides a reliable estimate of the radiative force even close to the wind sonic point. The CAK model therefore provides a good approximation for a solution obtained with non-Sobolev transfer. Below the sonic point, the CMF line force is significantly lower than the Sobolev one partly because of the strong gradients in the source function. This does not influence the mass-loss rate, as the wind mass-loss rate is set in the supersonic part of the wind below the critical point. However, when additional line broadening is present (e.g., the turbulent one) then the region of low CMF line force may extend outwards to the regions where the mass-loss rate is set. This results in a significant decrease in the wind mass-loss rate. We note that this is not a shortcoming of the Sobolev approximation because the Sobolev approximation is applicable to velocities higher than the turbulent velocity in this case.

The influence of turbulent line broadening may cause a dependence of the wind mass-loss rate on the atmospheric turbulent motions. Because theoretical models are not yet able to predict the atmospheric turbulent motions in hot stars in detail, we are unable to provide reliable wind mass-loss rate predictions until the theory of the atmospheric turbulence develops considerably (however see Cantiello et al. 2009, Aerts et al. 2009). Nowadays, hot star evolution seems to be a deterministic one depending only on the initial stellar parameters, i.e., mass, metallicity, and rotational rate. However, as the properties of atmospheric turbulent motions seem to be a non-trivial function of stellar parameters, the evolution of hot stars may become less deterministic, becoming instead dependent on free parameters describing the role of surface turbulence.

References

Abbott, D. C. 1980, ApJ, 242, 1183
Aerts, C., Puls, J., Godart, M., & Dupret, M.-A. 2009, A&A, 508, 409
Anderson, E., Bai, Z., Bischof, C. et al. 1999, LAPACK Users' Guide, 3rd ed. (SIAM, Philadelphia)
Asplund, M., Grevesse, N., & Sauval, A. J. 2005, in Cosmic Abundances as Records of Stellar Evolution and in Nucleosynthesis, ASP Conf. Ser. 336, ed. T. G. Barnes III, & F. N. Bash (ASP, San Francisco), 25
Bautista, M. A. 1996, A&AS, 119, 105
Bautista, M. A., & Pradhan, A. K. 1997, A&AS, 126, 365
Bouret, J.-C., Lanz, T., Hillier, D. J. et al. 2003, ApJ, 595, 1182
Bouret, J.-C., Lanz, T., & Hillier, D. J. 2005, A&A, 438, 301
Butler, K., Mendoza, C., & Zeippen, C. J. 1993, J. Phys. B., 26, 4409
Cantiello, M., Langer, N., Brott, I. et al. 2009, A&A, 499, 279
Castor, J. I. 1974, MNRAS, 169, 279

Castor, J. I. 2004, Radiation Hydrodynamics (Cambridge University Press, Cambridge)

Castor, J. I., Abbott, D. C., & Klein, R. I. 1975, ApJ, 195, 157 (CAK)

Chen, G. X., & Pradhan, A. K. 1999, A&AS, 136, 395

Cohen, D. H., Kuhn, M. A., Gagné, M., Jensen, E. L. N., & Miller, N. A. 2008, MNRAS, 386, 1855

Feldmeier, A., Puls, J., & Pauldrach, A. W. A. 1997, A&A, 322, 878

Feldmeier, A., Rätzel, D., & Owocki, S. P. 2008, ApJ, 679, 704

Fernley, J. A., Taylor, K. T., & Seaton, M. J. 1987, J. Phys. B, 20, 6457

Fullerton, A. W., Massa, D. L., & Prinja, R. K. 2006, ApJ, 637, 1025

Gayley, K. G. 2000, ApJ, 529, 1019

Gayley, K. G., Owocki, S. P., & Cranmer, S. R. 1995, ApJ, 442, 296

Gräfener, G., & Hamann, W.-R. 2005, A&A, 432, 633

Hamann, W.-R. 1981, A&A, 93, 353

Hillier, D. J., & Miller, D. L. 1998, ApJ, 496, 407

Howarth, I. D., Siebert, K. W., Hussain, G. A. J., & Prinja, R. K. 1997, MNRAS, 284, 265

Hummer, D. G., & Rybicki, G. B. 1985, ApJ, 293, 258

Hummer, D. G., Berrington, K. A., Eissner, W., et al. 1993, A&A, 279, 298

Korčáková, D., & Kubát, J. 2003, A&A, 401, 419

Kramer, R. H., Cohen, D. H., & Owocki, S. P. 2003, ApJ, 592, 532

Krtička, J., & Kubát, J. 2001, A&A, 369, 222

Krtička, J., & Kubát, J. 2004, A&A, 417, 1003 (Paper I)

Krtička, J., & Kubát, J. 2007a, in Active OB-Stars: Laboratories for Stellar & Circumstellar Physics, ed. S. Štefl, S. P. Owocki, & A. T. Okazaki (ASP, San Francisco), 153

Krtička, J., & Kubát, J. 2007b, A&A, 464, L17

Krtička, J., & Kubát, J. 2009, MNRAS, 394, 2065

Kubát, J. 1993, PhD thesis, Astronomický ústav AV ČR, Ondřejov

Kubát, J. 2003, in Modelling of Stellar Atmospheres, IAU Symp. 210, ed. N. E. Piskunov, W. W. Weiss & D. F. Gray (ASP, San Francisco), A8

Kudritzki, R. P., & Puls, J. 2000, ARA&A, 38, 613

Kudritzki, R.-P., Méndez, R. H., Puls, J., & McCarthy, J. K. 1997, in Planetary Nebulae, ed. H. J. Habing, & H. J. G. L. M. Lamers, Proc. IAU Symp., 180, 64

Kupka, F., Piskunov, N. E., Ryabchikova, T. A., Stempels, H. C., & Weiss, W. W. 1999, A&AS, 138, 119

Lanz, T., & Hubeny, I. 2003, ApJS, 146, 417

Lanz, T., & Hubeny, I. 2007, ApJS, 169, 83

Lucy, L. B. 2007, A&A, 468, 649

Luo, D., & Pradhan, A. K. 1989, J. Phys. B, 22, 3377

Marcolino, W. L. F., Bouret, J.-C., Martins, F., et al. 2009, A&A, 498, 837

Marigo, P., Girardi, L., Chiosi, C., & Wood, P. R. 2001, A&A, 371, 152

Markova, N., & Puls, J. 2008, A&A, 478, 823

Markova, N., Puls, J., Repolust, T., & Markov, H. 2004, A&A, 413, 693

Martins, F., Schaerer, D., Hillier, D. J., & Heydari-Malayeri, M. 2004, A&A, 420, 1087

Martins, F., Schaerer, D., Hillier, D. J., et al. 2005, A&A, 441, 735

Mihalas, D. 1978, Stellar Atmospheres (Freeman & Co., San Francisco)

Mihalas, D., & Hummer, D. G. 1974, ApJS, 28, 343

Mihalas, D., Kunasz, P. B., & Hummer, D. G. 1975, ApJ, 202, 465

Nahar, S. N., & Pradhan, A. K. 1993, J. Phys. B, 26, 1109

Nahar, S. N., & Pradhan, A. K. 1996, A&AS, 119, 509

Noerdlinger, P. D., & Rybicki, G. B. 1974, ApJ, 193, 651

Olson, G. L. 1982, ApJ, 255, 267

Oskinova, L. M., Hamann, W.-R., & Feldmeier, A. 2006, in G. Branduardi-Raymont, ed., High Resolution X-ray Spectroscopy, 27

Oskinova, L. M., Hamann, W.-R., & Feldmeier, A. 2007, A&A, 476, 1331

Owocki, S. P. 2004, in EAS Publications Series, Vol. 13, Evolution of Massive Stars, Mass Loss and Winds, ed. M. Heydari-Malayeri, Ph. Stee, & J.-P. Zahn, 163

Owocki, S. P., & Puls, J. 1999, ApJ, 510, 355

Owocki, S. P., Castor, J. I., & Rybicki, G. B. 1988, ApJ, 335, 914

Pauldrach, A., Puls, J., & Kudritzki, R. P. 1986, A&A, 164, 86

Pauldrach, A. W. A., Hoffmann, T. L., & Lennon, M. 2001, A&A, 375, 161

Pauldrach, A. W. A., Hoffmann, T. L., & Méndez, R. H. 2004, A&A, 419, 1111

Pavlakis, K. G., & Kylafis, N. D. 1996, ApJ, 467, 292

Piskunov, N. E., Kupka, F., Ryabchikova, T. A., Weiss, W. W., & Jeffery, C. S. 1995, A&AS, 112, 525

Puls, J. 1987, A&A, 184, 227

Puls, J., & Hummer, D. G. 1988, A&A, 191, 87

Puls, J., Markova, N., & Scuderi, S. 2008a, in Mass Loss from Stars and the Evolution of Stellar Clusters, ed. A. de Koter, L. Smith & R. Waters, (ASP, San Francisco), 101

Puls, J., Vink, J. S., & Najarro, F. 2008b, A&ARv, 16, 209

Repolust, T., Puls, J., & Herrero, A. 2004, A&A, 415, 349

Rybicki, G. B., & Hummer, D. G. 1978, ApJ, 219, 654

Sawey, P. M. J., & Berrington, K. A. 1992, J. Phys. B, 25, 1451

Schaller, G., Schaerer, D., Meynet, G., & Maeder, A. 1992, A&AS, 96, 269

Seaton, M. J. 1987, J. Phys. B, 20, 6363

Seaton, M. J., Zeippen, C. J., Tully, J. A., et al. 1992, Rev. Mexicana Astron. Astrofis., 23, 19

Sellmaier, F., Puls, J., Kudritzki, R. P. et al. 1993, A&A, 273, 533

Sobolev, V. V. 1947, *Dvizhushchiesia obolochki zvedz* (Leningr. Gos. Univ., Leningrad)

Sundqvist, J. O., Puls, J., & Feldmeier, A. 2010, A&A, 510, A11

Vink, J. S., de Koter, A., & Lamers, H. J. G. L. M. 2001, A&A, 369, 574

Woosley, S., & Heger, A. 2006, ApJ, 637, 914

Yoon, S.-C., & Langer, N. 2005, A&A, 443, 643

Zhang, H. L. 1996, A&AS, 119, 523

Zhang, H. L., & Pradhan, A. K. 1997, A&AS, 126, 373

Appendix A: The solution of CMF radiative transfer equation

To calculate the radiative force, the Mihalas et al. (1975) method for the solution of the CMF radiative transfer equation is modified in such a way that the v variable is specified on the spatial grid, and u on the intermediate one.

Following the notation of Mihalas et al. (1975), the depth index d increases inward, $r_1 = R_{\text{out}} > r_2 > \cdots > r_{\text{ND}} = R_*$, where R_{out} is the radius of the outer model boundary. The impact parameters p are labeled in order of increasing size by index j, $p_1 = 0 < p_2 < \cdots < p_{\text{NC}} < \cdots < p_{\text{NC+ND}}$, where NC is the number of rays intersecting the core. Along each ray with impact parameter p_j, we define grid in z and optical depth τ, $z_{j1} = \left(R_{\text{out}}^2 - p_j^2\right)^{1/2} > z_{j2} = \left(r_2^2 - p_j^2\right)^{1/2} > \cdots > z_{j,\text{NI}_j}$, where $\text{NI}_j = \text{ND}$ for $j \leq \text{NC}$, and $\text{NI}_j = \text{ND} + \text{NC} + 1 - j$ for $\text{NC} < j \leq \text{ND} + \text{NC}$, $\tau_{j1} = 0 < \tau_{j2} < \cdots < \tau_{j,\text{NI}_j}$. The frequencies are labeled by index k in order of decreasing values, $\nu_1 > \nu_2 > \cdots > \nu_{\text{NF}}$.

We assume that v is specified on the depth grid, and u is specified at intermediate grid points labeled by $d \pm \frac{1}{2}$. Suppressing the ray index j in the following, we define on each ray p_j

$$\chi_{k,d+1/2} = \frac{1}{2}\left[\chi(\nu_k, z_{d+1}) + \chi(\nu_k, z_d)\right], \tag{A.1}$$

$$\Delta\tau_{k,d+1/2} = \chi_{k,d+1/2}\left(z_d - z_{d+1}\right), \tag{A.2}$$

$$\Delta\tau_{k,d} = \frac{1}{2}\left(\Delta\tau_{k,d+1/2} + \Delta\tau_{k,d-1/2}\right). \tag{A.3}$$

The difference form of the system of the equations in Eq. (7) is

$$\frac{u(\nu_k, z_{d+1/2}) - u(\nu_k, z_{d-1/2})}{\Delta\tau_{k,d}} = v(\nu_k, z_d) + \frac{\gamma_{k,d}}{\Delta\nu_{k-1/2}}\left[v(\nu_k, z_d) - v(\nu_{k-1}, z_d)\right], \tag{A.4a}$$

$$\frac{v(\nu_k, z_{d+1}) - v(\nu_k, z_d)}{\Delta\tau_{k,d+1/2}} = u(\nu_k, z_{d+1/2}) - S(\nu_k, z_{d+1/2}) + \frac{\gamma_{k,d+1/2}}{\Delta\nu_{k-1/2}}\left[u(\nu_k, z_{d+1/2}) - u(\nu_{k-1}, z_{d+1/2})\right], \tag{A.4b}$$

where $d = 2, \ldots, \text{NI} - 1$, and

$$\Delta\nu_{k-1/2} = \nu_{k-1} - \nu_k, \tag{A.5}$$

$$\gamma_{k,d+1/2} = \frac{\alpha_{d+1/2}}{r_{d+1/2}\chi_{k,d+1/2}}\left(1 - \mu_{d+1/2}^2 + \beta_{d+1/2}\mu_{d+1/2}^2\right), \tag{A.6}$$

$$\gamma_{k,d} = \frac{\alpha_d}{r_d\chi_{k,d}}\left(1 - \mu_d^2 + \beta_d\mu_d^2\right). \tag{A.7}$$

Solving Eq. (A.4b) for $u(\nu_k, z_{d+1/2})$, we obtain

$$u(\nu_k, z_{d+1/2}) = \frac{v(\nu_k, z_{d+1}) - v(\nu_k, z_d)}{(1 + \delta_{k-1/2,d+1/2})\Delta\tau_{k,d+1/2}} + \frac{\delta_{k-1/2,d+1/2}}{1 + \delta_{k-1/2,d+1/2}}u(\nu_{k-1}, z_{d+1/2}) + \frac{S(\nu_k, z_{d+1/2})}{1 + \delta_{k-1/2,d+1/2}}, \tag{A.8}$$

where

$$\delta_{k-1/2,d+1/2} = \frac{\gamma_{k,d+1/2}}{\Delta\nu_{k-1/2}}. \tag{A.9}$$

Substituting Eq. (A.8) into Eq. (A.4a), we derive a linear system of equations for $v(\nu_k, z_d)$

$$\frac{1}{\Delta\tau_{k,d}}\left[\frac{v(\nu_k, z_{d+1})}{\Delta\tau_{k,d+1/2}(1 + \delta_{k-1/2,d+1/2})} - v(\nu_k, z_d)\left(\frac{1}{\Delta\tau_{k,d+1/2}(1 + \delta_{k-1/2,d+1/2})} + \frac{1}{\Delta\tau_{k,d-1/2}(1 + \delta_{k-1/2,d-1/2})}\right) + \right.$$
$$\left. \frac{v(\nu_k, z_{d-1})}{\Delta\tau_{k,d-1/2}(1 + \delta_{k-1/2,d-1/2})}\right]$$
$$= (1 + \delta_{k-1/2,d})v(\nu_k, z_d) - \frac{1}{\Delta\tau_{k,d}}\left(\frac{S(\nu_k, z_{d+1/2})}{1 + \delta_{k-1/2,d+1/2}} - \frac{S(\nu_k, z_{d-1/2})}{1 + \delta_{k-1/2,d-1/2}}\right) - \delta_{k-1/2,d}v(\nu_{k-1}, z_d) +$$
$$\frac{1}{\Delta\tau_{k,d}}\left[\frac{\delta_{k-1/2,d-1/2}u(\nu_{k-1}, z_{d-1/2})}{1 + \delta_{k-1/2,d-1/2}} - \frac{\delta_{k-1/2,d+1/2}u(\nu_{k-1}, z_{d+1/2})}{1 + \delta_{k-1/2,d+1/2}}\right]. \tag{A.10}$$

This system should be supplemented by equations corresponding to the boundary and initial conditions. At the outer spatial boundary z_{out}, we assume no infalling radiation, consequently $u = v$ and we derive from Eq. (7b)

$$\frac{1}{\chi(\nu, r)}\frac{\partial v(\nu, p, z)}{\partial z} - \gamma(\nu, p, z)\frac{\partial v(\nu, p, z)}{\partial \nu} = S(\nu, r) - v(\nu, p, z), \tag{A.11}$$

or, in a difference form

$$\frac{v(\nu_k, z_{d+1}) - v(\nu_k, z_d)}{\Delta\tau_{k,d+1/2}} = v(\nu_k, z_d)(1 + \delta_{k-1/2,d}) - \delta_{k-1/2,d}v(\nu_{k-1}, z_d) - S(\nu_k, z_d). \tag{A.12}$$

The infalling radiation at the inner boundary is taken from the model atmospheres. The initial solution for ν_1 is derived using the solution of the radiative transfer equation neglecting the velocity fields (Mihalas & Hummer 1974, Kubát 1993).

The velocity derivatives at the grid points are approximated as in the hydrodynamical code (see Krtička & Kubát 2001, Eq. (A.4a) therein). The derivatives in the middle points between grid points are calculated as the average of the derivatives at the grid points.

The system of algebraic equations Eq. (A.10) with boundary conditions is solved using the LAPACK package (`http://www.cs.colorado.edu/~lapack`, Anderson et al. 1999).